ISSN 8755-6839

SCIENCE OF **TSUNAMI HAZARDS**

Journal of Tsunami Society International

Volume 34 **Number 3** **2015**

ON THE FREQUENCY SPECTRUM OF TSUNAMI RADIATION

Frank C Lin[1,*], Kingkarn Sookhanaphibarn[1], Worawat Choensawat[1], George Pararas-Carayannis[2]

[1]Multimedia Intelligent Technology Laboratory, School of Science and Technology, Bangkok University, Rama 4 Rd, Khlong Toei, Bangkok 10110, Thailand

[2]Tsunami Society International, Honolulu, Hawaii 96815, USA

ABSTRACT

We have measured the spectrum of the tsunami radiation at the following wavelengths: 0.73 μm, 10.8μm, 12.0μm, 6.8μm and 3.8 μm (or 13,698 cm^{-1}, 925 cm^{-1}, 833 cm^{-1}, 1,470 cm^{-1} and 2,631 cm^{-1} in wave numbers). By comparing with infrared spectroscopic measurements of water, we are able to identify these transitions corroborating our hypothesis that the radiation originates from the transition of vibrational quantum energy levels of water molecules in aggregate. We have also repeated our previous study of the decay rate of tsunamis for a different tsunami. An estimate of the intensity of the tsunami radiation is made.

Keywords: *remote sensing, quantum mechanics, tsunami radiation, frequency spectrum, infrared spectroscopy, tsunami decay*

Vol. 34, No. 3, page 144 (2015)

**Corresponding author. Email: linbfrank@gmail.com. Tel/Fax: +662 612 4705*

1. INTRODUCTION

In previous studies [Lin *et al*, 2010; Lin and Sookhanaphibarn, 2011; Lin *et al.*, 2011; Lin *et al.*, 2012; Lin *et al.*, 2013; Lin *et al.*, 2014] we have reported our observation that a tsunami emits radiation at 11 μm which can be observed by a geostationary satellite in the infrared domain. In the present study we investigate the origin of this radiation by considering the molecular properties of water in its excited quantum states. Also in previous studies [Lin *et al.*, 2013; Lin *et al.*, 2014] we have experimentally determined the decay rate of a tsunami by exhibiting the time series of the tsunami signal (the pixel brightness) in hourly intervals. Here we shall extend our previous work by considering a different tsunami and measuring half hour intervals. Our result confirms our previous work. We also posit that the 0.73μm emission near the borderline of the spectral sensitivity of the human eye may present a spectacular show of nature.

2. QUANTUM PROPERTIES OF WATER

The water molecules in the ocean are nonlinear, triatomic molecules with the shape of an asymmetric top. There are three unequal moments of inertia about three mutually perpendicular principal axis. They are capable of executing both rotational and vibrational motion. There are three rotational modes and three vibrational modes. Rotational levels of water are labeled by the quantum numbers ($J\ K_a\ K_c$), where J is the quantum number for the total angular momentum. The indices K_a and K_c refer to the angular momentum quantum numbers in the corresponding prolate and oblate symmetric tops. In an environment with tetrahedral symmetry or higher, each ($J\ K_a\ K_c$) level is $2J+1$ fold degenerate, with an additional quantum number M_J which is the angular momentum projection on the axis *a* and *c*. The rotational states are correlated to the proton spin states through the Pauli principle: ortho-water states have total nuclear spin $I = 1$, and odd parity for $K_a + K_c$ in the ground vibrational state. The para-water states have total nuclear spin $I = 0$, and even parity for $K_a + K_c$ in the ground vibrational state [Beduz et al., 2012]. Photons are emitted when the molecules execute a transition from a higher vibrational quantum level to a lower level. These photons are mostly in the terahertz frequency range. For water, these spectra have been measured experimentally by several spectroscopic laboratories [Coudert *et al*., 2004; Coudert, 1994; Coudert, 1997; Languetin et al., 1999; Languetin et al., 2001; Toth, 1991; Toth, 1993]. These experimental spectroscopic measurements have been corroborated by theoretical calculations obtained by solving the Schrödinger equation with the appropriate Hamiltonian. Recently the range of vibrational and rotational energy levels has been greatly extended using variational calculations [Tennyson *et al*., 2001]. It should be noted that these levels may be subject to experimental errors. In the case of tsunamis, *the water molecules are in rapid motion and frequently collide violently with each other*. This circumstance may cause a shift in the quantum energy levels due to the centrifugal and Coriolius forces.

Tsunamis are perhaps one of the most destructive natural events on earth, comparable to volcanic eruptions or a meteorite striking the earth. In order to obtain an intuitive understanding of the scale of a tsunami event, we make an order of magnitude estimate of quantities of water, molecules, radiation and power released by such an event. At the onset of the tsunami event, a great mass of

water is transferred from the bottom of the ocean to the surface. The horizontal dimension of this great mass of water is circa 10 km x 10 km (2 pixels by 2 pixels). Following the estimate of Levin et al [Levin *et al*., 1998], we shall assume that the thickness of the water layer affected by the upward pulse to be 1.5 km. The total volume of water is therefore 1.5×10^{11} m^3. This amounts to a total number of molecules given by the astronomical number of 4×10^{36}.

The total power P radiated for a transition from k to i in a spectral line of frequency ν is

$$P_{line} = (4\pi)^{-1} h\nu \, A_{ki} \, N_k \tag{1}$$

where A_{ki} is the transition probability and
N_k is the number of exited atoms in level k.

Numerically A_{ki} is related to the line strength Z as follows [Martin and Wiese, 1996]

$$A_{ki} = \frac{2{,}026.1 \times 10^8}{\lambda^3 g_k} \times Z \approx 1 \times 10^8 \, Z \tag{2}$$

where

$$g_k = \sum_k (2J_k + 1) \tag{3}$$

is the statistical weight and λ the wavelength. If we substitute typical order of magnitude values for the quantities $h \approx 10^{-34}$, $\nu \approx 10^{12}$, $A_{ki} \approx 10^8$, $N_k \approx 10^{36}$ and $Z \approx 1$ into Eq. (1), we obtain for the total power $P_{line} \approx 10^{21}$ radiated per unit solid angle [Martin and Wiese, 1996; Tennyson *et al*., 2001].

Equation (1) is dominated by the number of molecules making the transition, which ultimately determines the intensity of the radiation that we were able to detect by the geostationary satellite. Although quantum transitions are microscopic events characterized by the Planck constant h, the immensity of the tsunami as characterized by the number of molecules involved, N_k, transforms it to a real world macroscopic phenomenon.

3. THE SATELLITE

The satellite that we utilized is the Japanese meteorological satellite MTSAT-2. This satellite is stationed at an altitude of approximately 36,000 km above the equator in a geostationary orbit at longitude 145˚ E. It is a 3-axis altitude controlled geostationary satellite with an advanced Himawari

Imager. There are five data channels at five different frequencies. These channels are capable of making multi-purpose imagery and wind derivation by tracking clouds and water vapor features. The resolution is from 0.5 to 2 km depending on the wavelength. The wavelength covers a range from 0.47 to 13.3 μm. The coverage is a full disk for every 10 minutes. The satellite carries a transponder to relay environmental data from the data collection platform. Data transmission rate is 18 GHz.

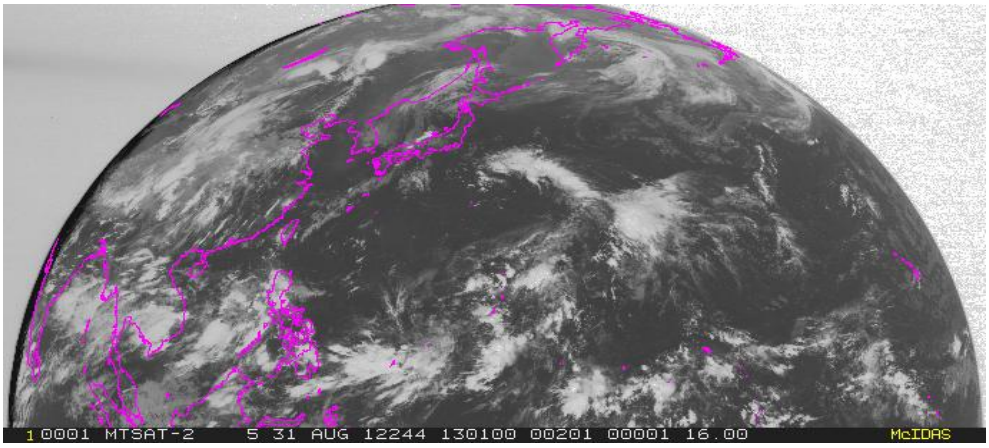

Fig. 1:MTSAT-2 satellite image on 2012-8-31 at 13:01 UTC at 3.75 microns

Under normal operations, the functions of the detectors are to record sea surface temperature, integrated water vapor, cloud cover, cloud top temperature etc. In our case we have shown [Lin *et al*, 2010; Lin and Sookhanaphibarn, 2011; Lin *et al.*, 2011; Lin *et al.*, 2012; Lin *et al.*, 2013; Lin *et al.*, 2014] that these detectors have also captured the tsunami radiation.

4. COMPARISON OF REMOTE SENSING AND SPECTROSCOPIC RESULTS

A seaquake of magnitude 7.6 on the Richter scale, positioned at latitude 10.8˚N and longitude 106.8˚E east of Soulangan, Philippines, took place at 12:48 UTC on 2012-08-31. In Table I we summarize the results obtained by examining satellite images from the MTSAT-2 taken on 2012-8-31 at 13:01 UTC. Images at the wavelengths 0.73 μm, 10.8 μm, 12.0 μm, 6.8 μm and 3.8 μm are recorded by the detectors of the satellite. In columns 1 and 2 of Table I we list the band and upper level quantum numbers from which the quantum transition took place. All transitions are to the ground level (0 0 0). The spectroscopic measurements reported by different authors are listed in column 5, which are compared with the frequencies detected by the satellite in column 4. We observe that they are overall compatible. The differences may be accounted for by the experimental errors of the satellite detectors and of the spectroscopic measurements, and by the shift in the spectral lines due to centrifugal and Coriolius forces. In addition, random translational motions of individual molecules leads to Doppler shift of absorption and emission wavelengths. We have only considered transitions to the ground state, although cascade transitions to higher levels (i.e. not to the ground state) are possible, and may have also been detected by the satellite [Toth, 1991; Toth, 1993; Lanquetin, 1999; Lanquetin, 2001]. The tsunami signal S is defined as the magnitude in pixels of the infrared radiation emitted by

the tsunami and measured directly from the satellite image [Lin *et al*, 2010; Lin and Sookhanaphibarn, 2011; Lin *et al.*, 2011; Lin *et al.*, 2012; Lin *et al.*, 2013; Lin *et al.*, 2014]. When referring to the satellite image, it is sometimes called the pixel brightness. A plot of the wavelength in microns versus the sine of the tsunami signal in pixels is shown in Fig.2.

Table 1: Spectroscopic & Satellite spectrum of H_2O at Soulangan at 13:01 UTC

Band	Upper Level $J\ K_a\ K_c$	λ μm	Satellite cm^{-1}	Spectroscopy cm^{-1}	S pixels	Reference
(030)	18 18 0	0.73	13,698	13,647	92	Coudert(2004)
(000)	7 4 4	10.8	925	927	258	Toth(1991)
(000)	7 3 4	12.0	833	842	173	Toth(1998)
(000)	9 5 5	6.8	1,470	1,474	209	Toth(1991)
(000)	13 5 8	3.8	2,631	2,629	119	Toth(1991)

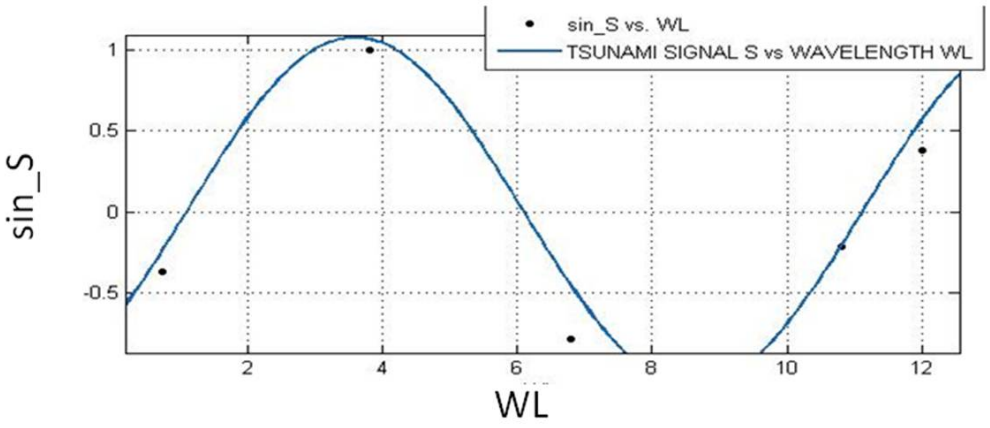

Fig.2: Sinusoidal behavior of tsunami signal vs. wavelength

The equation of interpolation is given below:

$$S = 1.076 * \sin(0.6256 * \lambda - 0.6703) \quad (4)$$

The parameters for the goodness of fit are: SSE: 0.1618, R-square: 0.916, and RMSE: 0.2844. This is solely an empirical relationship which suggests that the strength of the tsunami signal is not randomly distributed, (in which case we would obtain a scatter gram). We can interpret this relationship visually by considering Fig.3 in polar coordinates. If we equate the angle θ with the wavelength for the radiation detected by the satellite, λ, and the function f with the tsunami signal S, then we can conclude that the tsunami signal traces out the equipotential lines of a dipole for constant φ in the wavelength space (Fig.3). This diagram provides a graphical method for the calculation of the tsunami signal.

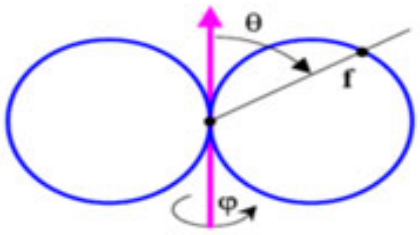

$$f\theta,\phi = A \cdot \sin^{f\theta}(\theta)$$

Fig. 3: Geometrical interpretation for tsunami signal S

5. Time Series and Decay of Tsunamis

On 2012-08-31 at 12:47:34 UTC a seaquake with moment magnitude of 7.6 with epicenter at latitude 10.8˚N and longitude 106.8˚E occurred 96 km. east of Soulangan, Philippines. According to the USGS, this seaquake was an intraplate event, which resulted from reverse faulting within the oceanic lithosphere in the region between the Philippines Sea plate and the Sunda plate. Tectonically, the Philippine Sea plate is bounded by the larger Pacific and Eurasian plates and the smaller Sunda plate. At the latitude of the seaquake, the Philippines Sea plate moves west northwestward at a velocity of approximately 10 cm/year with respect to the Sunda plate [Pararas-Carayannis, 2013]. The following figure show the MTSAT-2 infrared satellite image of the Philippines on 2012-08-31 at 10.8 μm at 13.01 UTC: This image is made just 13 min after the seaquake took place.

From this satellite image we make a cross-sectional cut from north to south along the longitude 106.8˚E and obtain the North-South signal diagram. The procedure to accomplish this is described in reference [Lin *et al.*, 2010; Lin *et al.*, 2014]:

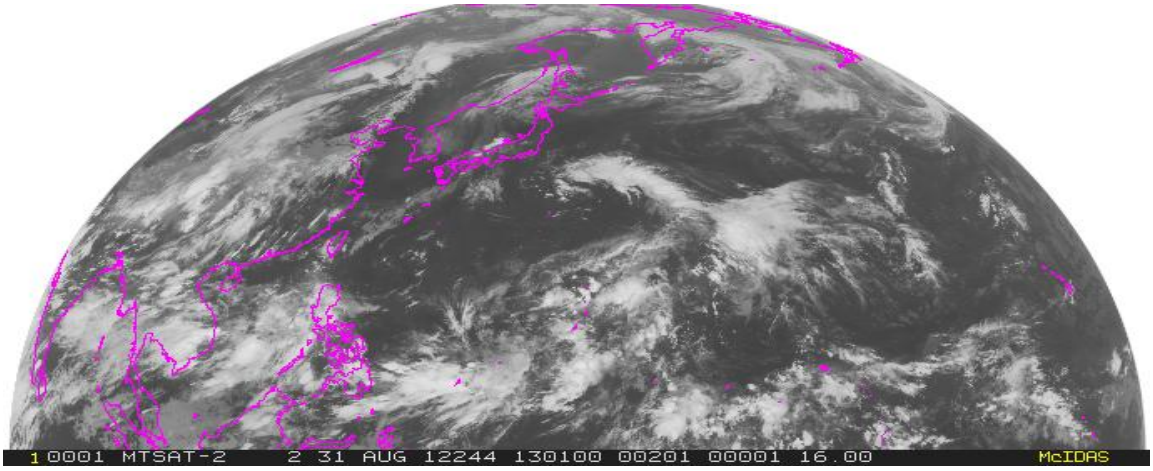

Fig. 4: Satellite image of Soulangan on 2012-08-31 at 13:01 UTC and wavelength 10.8 µm

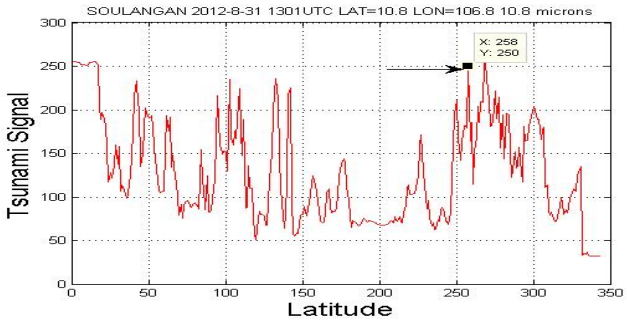

Fig.5: North-South signal diagram for Soulangan on 2012-8-31 at 13.01 UTC for 10.8µm

An arrow points to the tsunami signal at latitude 10.8˚ or 258 pixels. A similar diagram can be constructed for a cut along the East-West axis (i.e. along 10.8˚E latitude, which we call the East-West signal diagram).

In order to construct a Time Series to investigate the rate of decay of the tsunami signal, we have measured the signal at 13:01, 13:32, 14:01, 15:01 and 16:01 UTC, and for the five available frequencies 0.73, 3.8, 6.8, 10.8 and 12.0 µm. The result is summarized in Table 2 in Appendix A. In the following we discuss the decay pattern of each of these channels.

A. The IR-4 channel:

At 10.8 μm, this is the long wave length or IR-C (also classified as IR-4) band, which is the band utilized in our previous investigations [Lin *et al*, 2010; Lin and Sookhanaphibarn, 2011; Lin *et al.*, 2011; Lin *et al.*, 2012; Lin *et al.*, 2013; Lin *et al.*, 2014]. The IR photon energy is between 0.001 and 1.7 eV. This is the atmospheric window covered by detectors such as HgCdTe and microbolometers. Satellite images in this frequency region can be used to determine cloud heights and types, to calculate land and surface water temperatures, and to locate ocean surface features. These infrared pictures are also used to depict ocean eddies or vortices and map currents. And, as we have demonstrated in our previous work, it can be used to detect tsunami signals. Fig. 6 shows the Time Series for Tsunami Signal for 10.8 μm.

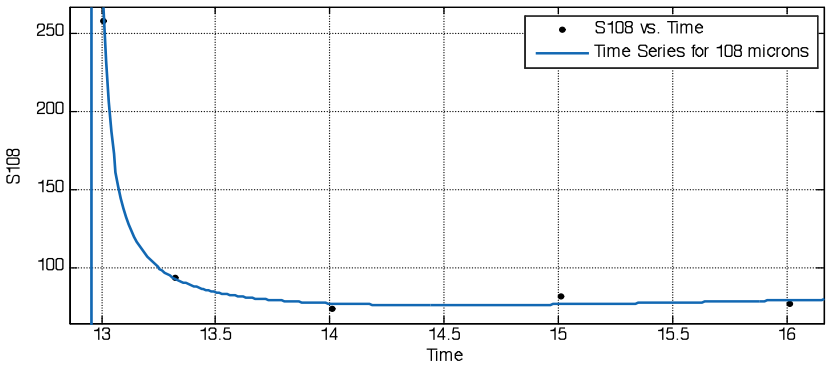

Fig. 6: Time series for tsunami signal for 10.8 μm

We observe that the signal has decayed by approximately ¾ after half an hour's time has lapsed and remained at that level. There is no rebound within a period of three hours, indicating that the tsunami effect has dissipated.

B. The IR-5 Channel:

The following figure, Fig.7, shows the Time Series for 12.0 μm, which is also in the IR-C band (IR-5). The behavior is similar to the previous case, although there is a steady rise of the tsunami signal with time. Since we do not observe this behavior with the other channels, it is likely that it is not directly associated with the tsunami.

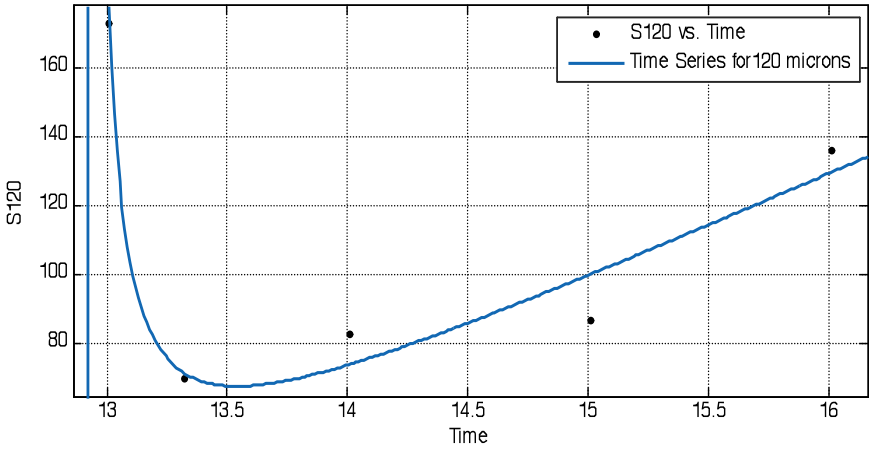

Fig. 7: Time series for tsunami at 12.00 µm.

C. The Water Vapor channel at 6.75 µm:

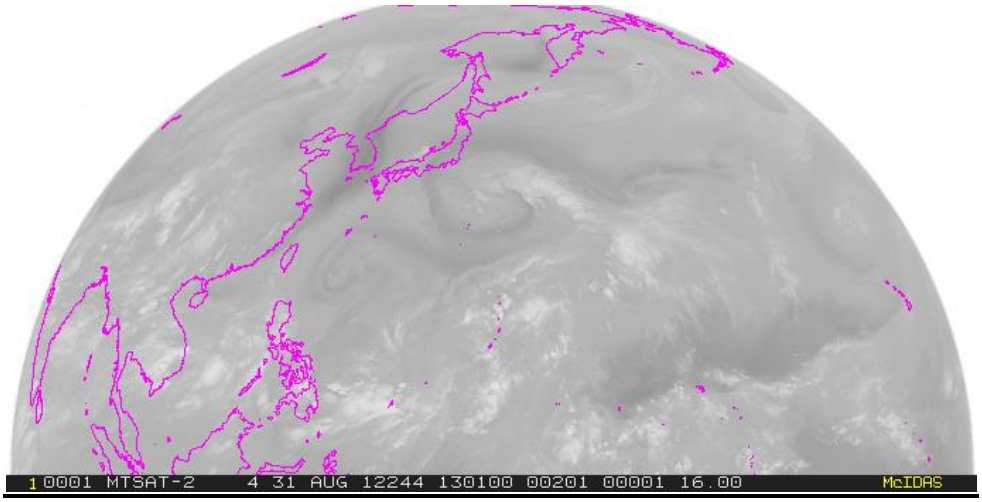

Fig. 8: MTSAT-2 satellite image of Soulangan at 13:01 UTC at 6.75 µm

The water vapor channel (from 6.40 to 7.08 µm) shows the amount of moisture in the atmosphere. This channel is the most important IR absorber. Fig. 9 shows the time series at 6.75 µm. We note that the band around 6.3 µm (1590 cm^{-1}) is due to the H-O-H bending vibration.

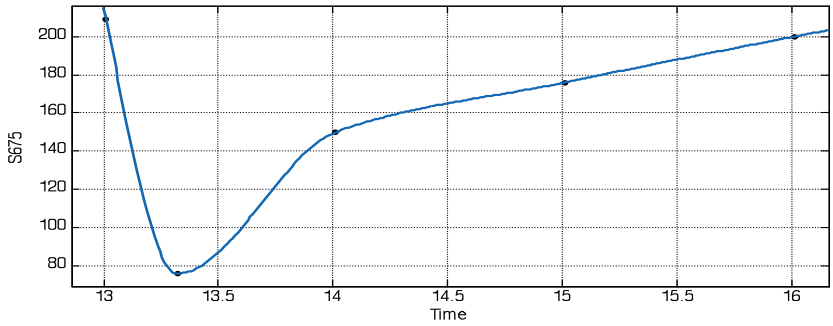

Fig. 9: Time series of tsunami for water vapor channel

We observe that the tsunami signal starts to rise half an hour after the onset of the tsunami and continues this trend, albeit at a slow rate of change. This behavior suggests that immediately after the decay the moisture content of the atmosphere begins to unravel due to local atmospheric variations possibly due to wind and that the tail of the Time Series is not directly related to the tsunami *per se*. This implies that the water vapor channel is a poor choice for the observation of the tsunami signal.

D. The Intermediate Infrared Channel:

The intermediate infrared channel (IIR) at 3.75 μm also belongs to the IR-C band in the infrared spectrum. This band is used for tracking, for example, by heat seeking missiles. The Time Series, as shown in Fig.10, shows the typical behavior of tsunami decay. The decay occurs within half an hour, and then maintains a constant nadir. This channel is therefore suitable for investigating tsunami onsets.

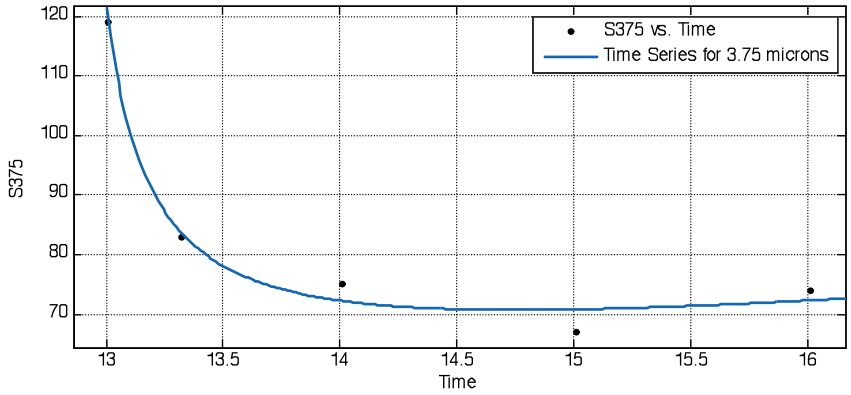

Fig.10 Time series for the 3.75 μm channel

E. The Near Infrared Band:

This relatively higher frequency channel is in the Near Infrared (IR-A) spectra range which is characterized by water absorption, and commonly used in fiber optic telecommunication because of low attenuation losses in the SiO_2 glass. It is at the borderline of detection by the human eye since it is closest to the visible spectrum.

However, since the transition took place from a relatively high level, (0 3 0), to the ground state, the transition probability will be weaker and the intensity of radiation will be reduced (see Table I). The Schrödinger wavefunction ψ for the water molecule in this excited state is given by a linear combination of the symmetric O-H stretch, v_1, and the antisymmetric stretch v_3: $\psi = av_1 + bv_3$, where a and b are constants. The bending contribution v_2 is not present. We speculate that the tsunami onset may be observable by a passenger in a ship inadvertently navigating in the vicinity. If visible at all, he would perceive the event as a burst of dull, deep red afterglow, extending approximately for 10 km in every direction, and disappearing within half an hour. It could be one of the most spectacular displays of nature. This is therefore another suitable channel for the investigation of tsunamis.

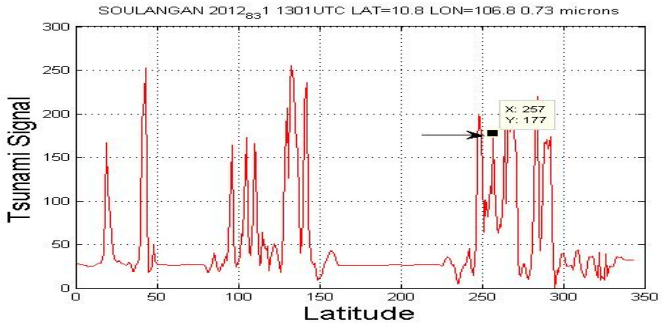

Fig. 11: North-South signal diagram for Soulangan at 13:01 UTC on 2012-8-31 at 0.73 microns

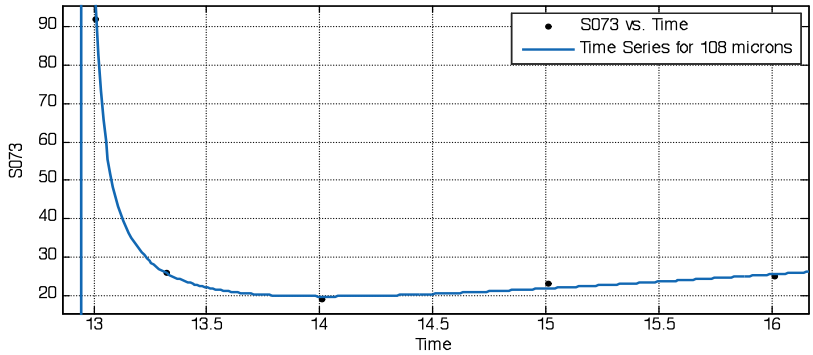

Fig.12: Time series for the 0.73 μm channel

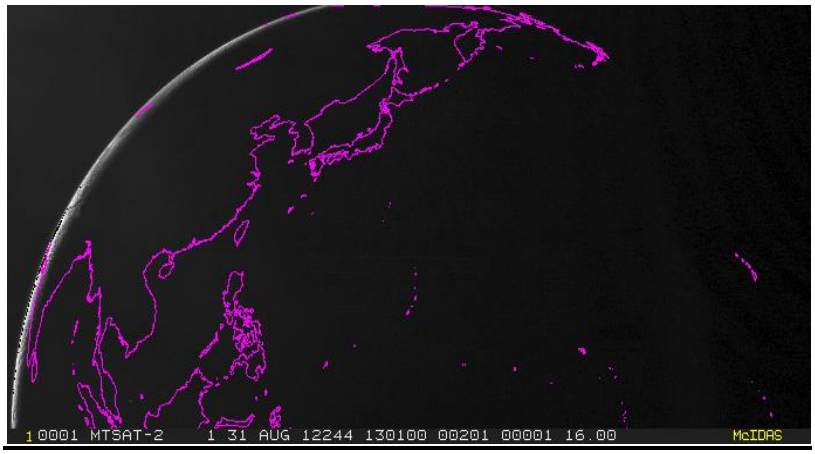

Fig. 13: MTSAT-2 satellite image of Soulangan 2012/8/31 13:01 UTC at 0.73 microns

In the above, Fig.11 shows the North-South signal diagram, Fig. 12 the time series, and Fig.13 the MSAT-2 satellite image for this channel.

6. Conclusion

We conclude as follows:

1) We have demonstrated experimentally that the tsunami radiates at all frequencies in the infrared range and decays within half an hour. We suggest that the eye of the tsunami may be visible to the naked human eye since it emits radiation at 0.73 μm which is at the borderline of spectral sensitivity.

2) We have shown that the infrared radiation detected by the geostationary satellite can be accounted for by transitions between vibrational quantum levels of water molecules. We cannot exclude, however, the possibility that another source of radiation may also be present. Novik *et al.* [2014] have shown that, on the basis of a 3D model, a moving oceanic lithosphere can generate electromagnetic disturbances and after propagation to the earth surface emit radiation into the atmosphere. However, the frequency interval predicted by this mechanism is not in the infrared range. Some impurities in the ocean, such as sand (SiO_2), are capable of emitting infrared radiation but they are quantitatively insignificant. Among the quake precursor events is often a special cloud formation above the stress area of a potential fracture of a fault. It appears that precursory stresses (perhaps of electromagnetic nature and resulting friction and Coulomb stress), among other precursor events (radon, hydrogen emissions, etc), break down the water of hydration in the hard rocks, or perhaps affect the water molecules of the sea by breaking their hydrogen bonding that holds them together. Love and Raleigh seismic surface waves may play a role on altering the quantum state of the sea water molecules, thus

resulting in the release of photons or other infrared radiation. We are not aware of interference by other molecules in the atmosphere (CO_2, N_2, water droplets etc) at these frequencies. It is likely that the tsunami broadcasts infrared radiation at many different frequencies corresponding to transitions from many different rotational-vibrational quantum energy levels, and that we have only, *par hasard*, measured five of these by our satellite. In view of the richness of the molecular spectra of water, it is not unjustified to hypothesize that the tsunami is playing a symphony with many chords.

7. APPENDIX A

Table 2: Time series & frequency dependence of tsunami radiation

Location	**Sat**	**Lat N**	**Lon E**	**Date**	**Image Time**	λ μm	**M_e**	S^1 pixels	**REM**
Soulangan	MTSAT2	10.8	106.8	2012_8_31	13:01	3.75	7.6	119	Low cloud
Seaquake at 12:48UTC						12.0		173	Cloud temp
						10.8		258	Cloud top
						0.73		92	Surface feature
						6.75		209	WV
	MTSAT2				13:32	3.8		83	
						12.0		70	
						10.8		94	
						0.73		26	
						6.8		76	
	FY2E				14:01	3.8		None*	
						12.0		83	
						10.8		74	
						0.73		19	
						6.8		150	
	MTSAT2				15:01	6.8		176	
						12.0		87	
						3.8		67	
						10.8		82	
						0.73		23	
	MTSAT2				16:01	6.8		200	
						12.0		136	
						3.8		74	
						10.8		77	
						0.73		25	

*Cancelled due to eclipse. An average value is used. [1]measured by East West Signal

REFERENCES

Beduz, C, M.Carravetta, J. Y. C. Chen, M. Concistre, M. Denning, M. Frunzi, A. J. Horsewill, O. G. Johannessen, R. Lawler, X. Lei, M. H. Levitt, Y. Li, S. Mamone, Y. Murata, U. Nagel, T. Nishida, J. Ollivier, S. Rols, T. Rööm, R. Sarkar, N. J. Turro, Y. Yang, 2012. Quantum rotation of *ortho* and *para*-water encapsulated in a fullerene cage: Proceedings of the National Academy of Science 109, pp. 12894-12898.

Coudert, L.H., 1994. Analysis of the Rotational Levels of Water and Determination of the Potential Energy Function for the Bending ν_2 Mode: J. of Mol. Spectroscopy 165, pp.406-425.

Coudert, L.H., 1997. Analysis of the Line Positions and Line Intensities in the ν_2 Band of the Water Molecule: J. of Mol. Spectroscopy 181, pp.246-273

Coudert, L.H., O.Pirali, M.Vervloet, R.Languetin and C.Camy-Peyret, 2004. The eight first vibrational states of the water molecule: measurement and analysis. J. of Molecular Spectroscopy 228, pp. 471-498.

Lanquetin, R., L.H.Coudert and C.Camy-Peyret, 1999. High-Lying Rotational Levels of Water: Comparison of Calculated and Experimental Energy Levels for (0 0 0) and (0 1 0) up to J=25 and 21. J. of Mol. Spectroscopy 195, 54-67.

Lanquetin, R., L.H.Coudert and C.Camy-Peyret, 2001. High-Lying Rotational Levels of Water: An Analysis of the Energy Levels of the Five Vibrational States: J. of Mol. Spectroscopy 206, 83-103.

Levin B.V., M.A.Nosov, V.P.Pavlov and L.N.Rykunov, 1998. Cooling of the Ocean Surface as a Result of Seaquakes. Doklady Earth Sciences Vol.358, No.1, pp. 132-135.

Lin F.C., K. Na Nakornphanom, K. Sookhanaphibarn, and C. Lursinsap, 2010. "A New Paradigm for Detecting Tsunamis by Remote Sensing"; International Journal of Geoinformatics, Vol.6, No.1, March 2010, pp.19-30.

Lin F.C. and K. Sookhanaphibarn, 2011. Representation of Tsunamis in Generalized Hyperspace: Proceedings of the IEEE International Geoscience and Remote Sensing Symposium (IGARSS'11), Sendai/Vancouver, July 21, 2011. pp. 4355-4358.

Lin F.C., W. Zhu and K. Sookhanaphibarn, 2011. Observation of Tsunami Radiation at Tohoku by Remote Sensing, Science of Tsunami Hazards, Vol.30, No.4,Honolulu, HI, December 2011, pp. 223-232.

Lin, F.C., W. Zhu and K. Sookhanaphibarn, 2012. A Detail Analysis of the Tohoku Tsunami by Remote Sensing, Proceedings of the IEEE International Geoscience and Remote Sensing Symposium (IGARSS'12), Munich, Germany, pp.1166-1169.

Lin. F.C., W. Zhu, K. Sookhanaphibarn and P. Silapasuphakornwong, 2013. REMOTE:-A Satellite Based Tsunami Early Warning Detection System, Proceedings of the IEEE International Geoscience and Remote Sensing Symposium (IGARSS' 13), Melbourne, Australia, pp. 3694-3697.

Lin, F.C., K. Sookhanaphibarn, V. Sa-yakanit and G. Pararas-Carayannis, 2014. REMOTE: Reconnaissance & Monitoring of Tsunami Events, Science of Tsunami Hazards, Vol.33, No.2, pp.86-111

Martin, W.C. and W.L.Wiese, 1996. Atomic, Molecular and Optical Physics Handbook, G.W.R.Drake, Ed., AIP Press, Woodbury, N.Y.

Novik, O., S. Ershov, Y. Ruzhin, F. Smirnov and M. Volgin, 2014. Theory and detection scheme of seismic EM signals transferred into the atmosphere from the oceanic and continental lithosphere. Advances in Space Research 54, pp. 168-184.

Pararas-Carayannis, G., 2013. "The Great Tohoku-Oki Earthquake and Tsunami of March 11, 2011 in Japan: A Critical Review and Evaluation of the Tsunami Source Mechanism," Pure and Applied Geophysics, pp. 1-22.

Tennyson, J., N.F. Zobov, R. Williamson, O.L. Polyansky, P.F. Bernath, 2001. Experimental energy levels of the water molecule. Journal of Physical and Chemical Reference Data, 30 (3). pp. 735-831.

Toth, R. A., 1991. ν_2 band of $H_2{}^{16}O$: line strengths and transition frequencies. J. Opt. Soc. Am. B, Vol.8, No.11, November 1991, pp.2236-2255.

Toth, Robert A., 1993. $2\nu_2 - \nu_2$ and $2\nu_2$ bands of $H_2{}^{16}O$, $H_2{}^{17}O$ and $H_2{}^{18}O$: Line Positions and Strength: J. Opt. Soc. Am. B, Vol.10, No.9, September 1993, pp. 1526-1544.

ISSN 8755-6839

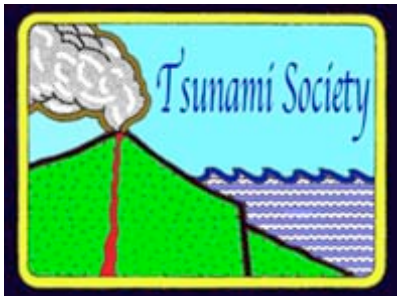

SCIENCE OF **TSUNAMI HAZARDS**

Journal of Tsunami Society International

Volume 34 **Number 3** **2015**

TSUNAMI SOCIETY INTERNATIONAL, 1741 Ala Moana Blvd. #70, Honolulu, HI 96815, USA.

WWW.TSUNAMISOCIETY.ORG